First-Principles-Based Multiphysics Modeling and Simulation of On-Chip Cu-Graphene Hybrid Nanointerconnects in Comparison With Simplified Model-Based Analysis

Shuzhan Sun, *Graduate Student Member, IEEE*, and Dan Jiao, *Fellow, IEEE*

***Abstract*—Cu-Graphene (Cu-G) hybrid nanointerconnects, as well as many graphene-based devices, have a potential to significantly advance the technology of on-chip integrated circuits (IC). However, their modeling and simulation for a long time has relied on simplified steady-state models of graphene. To examine the validity and accuracy of existing simplified models in high-frequency and subnanometer applications, in this article, we theoretically analyze the assumptions made in existing simplified models. Meanwhile, we develop a first-principles-based multiphysics modeling and simulation algorithm to numerically assess the accuracy of the simplified model-based analysis of Cu-G interconnects. In this algorithm, the Maxwell's equations, the equation characterizing graphene, and the Boltzmann equation are cosimulated in time domain. A significant difference is observed between the first-principles-based analysis and the simplified model-based one when the frequency is high or/and the dimension of the Cu-G structure is small, which necessitates the first-principles-based multiphysics modeling and simulation for the design of advanced Cu-G interconnects.**

***Index Terms*—Boltzmann equation, cu-graphene hybrid nanointerconnects, Drude model, finite difference methods, hybrid integrated circuits, Maxwell's equations, multiphysics modeling and simulation, time-domain analysis.**

I. Introduction

EVER since first being fabricated in the laboratory, graphene has attracted a lot of attentions in the design of integrated circuits (ICs). Due to graphene's 2-D nature, μm-long mean free path, high physical strength, and large electrical and thermal conductivity, graphene has a potential to push the next-generation ICs to an era of ultrascaled dimension, lower signal delay, faster data transferring speed, reduced energy consumption and heat generation, and better reliability [1]. Over the last decade, utilizing these advantages of graphene, researchers have proposed many graphene-based on-chip designs, including pure graphene-based interconnects and nanoscale functional devices, and Cu-Graphene (Cu-G) hybrid structures like graphene encapsulated Cu interconnects. However, the electrical performance of general on-chip Cu-G hybrid interconnects remains unclear at high operating frequencies ($\sim$100 GHz or higher) and in the sub-10 nm regime. On the one hand, the fabrication and measurement capability is limited. In most laboratories, only single Cu-G hybrid structure can be measured at either dc or an optical frequency. Thus, existing experimental capabilities are not sufficient to measure the performance of complicated on-chip Cu-G hybrid systems at desired frequencies. On the other hand, most of existing simulation methods, which separately model the graphene layers [2]–[4] and the hybrid Cu-G structure [5]–[8], may have accuracy problems in high frequency and subnanometer (nm) simulations.

The limited accuracy of existing simplified model-based simulation methods is mainly due to three factors. First, most of simplified graphene models are inaccurate at high frequencies. For example, the model in [2] gives the conductivity of graphene layer by counting the number of conduction channels. However, it only considers a graphene length shorter than the mean free path (MFP) and it fails to model the frequency dependence. Another widely used model of graphene is Kubo formula [3], which has considered both the intraband and interband transition. The intraband transition of Kubo formula corresponds to the Drude model [9]–[12] in this article and will be discussed in detail in Section II. Second, Ohm's law itself can be inaccurate because the skin depth becomes comparable to the MFP of graphene at high frequencies [9]. When the skin depth becomes comparable to the MFP of graphene, the carriers can no longer be considered to move under the influence of a constant field between collisions, and the current at any point is also influenced by the electric fields at other points. This renders the assumption of Ohm's law invalid and necessitates a more generic approach using the Boltzmann equation. Thus, any conductivity model extracted with Ohm's law is not accurate. Third, existing decoupled electrical conductivity models of graphene assume graphene's steady state responses to an external stimulus. This assumption can be valid for many low frequency applications, but it is unlikely to hold true in high-frequency settings. The main reason to the failure at high frequencies is the low back scattering frequency (BSF) of graphene ($\sim$100 GHz) [13], [14]. When the

Manuscript received September 3, 2019; revised November 10, 2019; accepted December 18, 2019. Date of publication January 7, 2020; date of current version February 10, 2020. This work was supported by the National Science Foundation under Grant 1619062. This article is an expanded version from the IEEE MTT-S International Conference on Numerical Electromagnetic and Multiphysics Modeling and Optimization, Cambridge, MA, USA, May 29–31, 2019. *(Corresponding author: Dan Jiao.)*

The authors are with the School of Electrical and Computer Engineering, Purdue University, West Lafayette, IN 47907 USA (e-mail: sun630@purdue.edu; djiao@purdue.edu).

Digital Object Identifier 10.1109/JMMCT.2020.2964655

signal frequency in Cu-G interconnects becomes high enough to reach the relatively low BSF of graphene, graphene layers may not have enough scatterings to re-equilibrate themselves. As a result, it may not give the physical steady state response predicted by the steady-state conductivity models. Since the decoupled steady-state models can miss graphene's dynamic responses at high frequencies, a first-principles-based dynamic modeling and simulation in the time domain is needed.

In our conference paper [15], we develop a multiphysics-based model and an efficient simulation algorithm to co-simulate directly in the time domain the Maxwell's equations, equations characterizing graphene materials, and the Boltzmann equation from dc to high frequencies. A detailed description of the algorithm is given in [16]. In this article, we study the difference between the first-principles-based method of [15] and commonly used simplified models such as the Drude-model-based approach for analyzing general on-chip Cu-G hybrid systems, from both theoretical and numerical perspectives. To do so, we first develop a Drude-model-based simulation algorithm, including the derivation of the Drude model from the Boltzmann transport equation, the numerical representation of the Drude model, and an efficient algorithm for simulating the Drude model in conjunction with the finite difference time domain (FDTD) to analyze a Cu-G interconnect. We, then, compare it with the first-principles-based multiphysics model and the resulting simulation algorithm both theoretically and numerically through extensive numerical experiments performed on the Cu-G nanointerconnects. We find that the first-principles-based analysis is necessary to capture the physical process happening in a Cu-G interconnect at microwave frequencies and in the sub-nm regime.

II. Simplified Model-Based Simulation Algorithm for Analyzing On-Chip Cu-G Hybrid Interconnects

Graphene has been extensively simulated via various models in last decade. Among these models, Drude model [9]–[12], within the framework of Boltzmann transport theories, is a widely used model and has shown good accuracy in a linear regime. In this section, we derive Drude model from the Boltzmann transport equation. We, then, present a numerical algorithm to apply the Drude model to simulate Cu-G hybrid interconnects in the time domain.

A. Analytical Derivation of Drude Model From the Boltzmann Transport Equation

The distribution function of charge carriers in graphene, denoted by $f(\mathbf{r},\mathbf{k},t)$ in phase space (real $\mathbf{r}$-space and momentum $\mathbf{k}$-space), is governed by the following Boltzmann transport equation:

$$\mathbf{v}\cdot\nabla_{\mathbf{r}}f+\frac{q}{\hbar}\mathbf{E}\cdot\nabla_{\mathbf{k}}f+\frac{\partial f}{\partial t}=-\frac{f-f_0}{\tau} \tag{1}$$

where $\mathbf{v}=d\mathbf{r}/dt$ is the velocity vector, $\mathbf{k}=\mathbf{p}/\hbar$ is the wave vector of Bloch wave in momentum space, q is the amount of charge in each carrier, $\mathbf{E}$ is the electric field intensity, and $\hbar$ is the Planck constant. The scattering term on the right-hand side of (1) is approximated by the relaxation time approximation [17], where τ is the relaxation time, and f_0 is the Fermi–Dirac distribution at the equilibrium state as the following:

$$f_0=\left[1+\exp\left(\frac{\xi-\xi_{\mathrm{F}}}{k_{\mathrm{B}}T}\right)\right]^{-1} \tag{2}$$

in which ξ is the carrier's energy, ξ_{F} is the Fermi energy (also called Fermi level or chemical potential), k_{B} is the Boltzmann constant, and T is the temperature.

Given $f(\mathbf{r},\mathbf{k},t)$, the conduction current density $\mathbf{j}_g$ in graphene can be evaluated from an integration over $\mathbf{k}$-space as

$$\mathbf{j}_g=\frac{g_s g_v q}{(2\pi)^d}\int_{\mathbf{k}} f\mathbf{v}d\mathbf{k} \tag{3}$$

where g_s and g_v are spin, and valley degeneracy, respectively, and d denotes the problem dimension, which is 2 and 3 in a 2-, and 3-D analysis, respectively. In order to calculate $\mathbf{j}_g$ from (1) and (3), the velocity vector $\mathbf{v}$ needs to be expressed as a function of $\mathbf{k}$. Semiclassically, by treating the Bloch waves as wave packets, the classical velocity $\mathbf{v}$ is defined as the group velocity $d\omega/d\mathbf{k}$ of such wave packets [17]. The frequency ω is associated with a wave function of energy ξ by quantum theory, $\omega=\xi/\hbar$, and hence, $\mathbf{v}=\nabla_{\mathbf{k}}\xi/\hbar$. After substituting the following linear dispersion relation of graphene [18]:

$$\xi=v_{\mathrm{F}}\hbar k \tag{4}$$

where $v_{\mathrm{F}}=10^6$ m/s is the Fermi velocity and $k=\sqrt{k_x^2+k_y^2}$, we can express the velocity vector $\mathbf{v}$ as the following function of $\mathbf{k}$:

$$\mathbf{v}(\mathbf{k})=\nabla_{\mathbf{k}}\xi/\hbar=v_{\mathrm{F}}\hat{\mathbf{k}}. \tag{5}$$

To obtain the analytical Drude model of graphene from Boltzmann transport equation (1), three assumptions are made as follows.

1) The spatial variance of f is small, thus $\mathbf{v}\cdot\nabla_{\mathbf{r}}f\sim 0$.
2) The external fields are small, leading to a small change of the Fermi sea. Thus, $f\sim f_0$ in $\mathbf{k}$-space and $\frac{q}{\hbar}\mathbf{E}\cdot\nabla_{\mathbf{k}}f\sim\frac{q}{\hbar}\mathbf{E}\cdot\nabla_{\mathbf{k}}f_0$.
3) The nonlinear effect is negligible, thus, $\frac{\partial f}{\partial t}$ can be analyzed in the frequency domain using $j\omega\tilde{f}$.

Denoting $\tilde{f}$ and $\tilde{\mathbf{E}}$ as the frequency domain counterparts of $f(t)$ and $\mathbf{E}(t)$, the aforementioned three assumptions lead to a simplified Boltzmann transport equation in frequency domain as follows:

$$\frac{q}{\hbar}\tilde{\mathbf{E}}\cdot\nabla_{\mathbf{k}}f_0+j\omega\tilde{f}=-\frac{\tilde{f}-f_0}{\tau} \tag{6}$$

from which we can get an analytical expression of charge carrier distribution

$$\tilde{f}=\frac{1}{1+j\omega\tau}\left(f_0-\frac{\tau q}{\hbar}\tilde{\mathbf{E}}\cdot\nabla_{\mathbf{k}}f_0\right). \tag{7}$$

Substituting the analytical $\tilde{f}$ in (7) and velocity $\mathbf{v}$ in (5) into (3), we obtain an analytical expression of conduction current density

$\tilde{\mathbf{j}}_g$ in graphene

$$\tilde{\mathbf{j}}_g = \frac{\tilde{\mathbf{E}}}{1+j\omega\tau} \cdot \frac{\tau q}{\hbar}\frac{g_s g_v q}{(2\pi)^d} v_{\mathrm{F}} \int_{\mathbf{k}} (-\nabla_{\mathbf{k}} f_0)\hat{\mathbf{k}} d\mathbf{k} = \frac{\sigma_{\mathrm{dc}}\tilde{\mathbf{E}}}{1+j\omega\tau} \tag{8}$$

with

$$\sigma_{\mathrm{dc}}\mathbf{I} = \frac{\tau q}{\hbar}\frac{g_s g_v q}{(2\pi)^d} v_{\mathrm{F}} \int_{\mathbf{k}} (-\nabla_{\mathbf{k}} f_0)\hat{\mathbf{k}} d\mathbf{k}. \tag{9}$$

Here, we have used the symmetry of the linear dispersion and the spherical Fermi sphere to simplify the integration. First, the integration of $f_0\mathbf{v}$ is 0 because f_0 is an even function in $\mathbf{k}$-space while $\mathbf{v}$ is an odd function. Second, the tensor $\int_{\mathbf{k}}(-\nabla_{\mathbf{k}} f_0)\hat{\mathbf{k}} d\mathbf{k}$ is isotropic due to the symmetry, thus, can be written as a scaled identity matrix. As a result of the three assumptions and the use of special symmetry, graphene follows Ohm's Law as shown in (8).

The analytical Drude model derived in the above-mentioned equation yields the conductivity of graphene in frequency domain

$$\tilde{\sigma}_g(\omega) = \frac{\sigma_{\mathrm{dc}}}{1+j\omega\tau} \tag{10}$$

where ω is angular frequency, τ is the relaxation time as that in Boltzmann equation (1), and σ_{dc} is the dc conductivity of graphene. From the open literature, it can be seen that σ_{dc} can be obtained in many ways, such as represented as (9) by utilizing the dispersion relation, represented by other parameters like the carrier density [12], and directly measured at low frequencies [11]. For the comparison concerned in this article between a first-principles-based simulation and the Drude-model-based simulation, in order to use the same assumptions and parameters, σ_{dc} in Drude model is extracted from the numerical Boltzmann solver developed in this article.

Drude model (10) agrees with the intraband transition part of Kubo formula [3], which is a more accurate conductivity model of graphene accounting for both the intraband and interband transition. The intraband transition, as described by the above-mentioned Boltzmann transport equation (1) and Drude model (10), is the transition of electron states near the Fermi surface in $\mathbf{k}$-space. The interband transition, corresponding to the electrons poping up from an inner band to an upper conduction band, can be obtained by employing the Kramers–Kronig relation or Fermis golden rule [19]. For ICs, the intraband transition is the dominant effect because both thermal excitation energy ($T = 300$ K, $k_{\mathrm{B}}T \sim 25$ meV) and photon energy ($\omega = 10$ GHz, $\hbar\omega \sim 6.6 \times 10^{-6}$ eV) are much smaller than the Fermi energy of graphene (typically 0.21 eV). The electrons at an inner band can hardly find enough excitation energy to pop up to an upper band, thus, the interband transition is suppressed. In this article, focusing on simulating on-chip Cu-G interconnects, we only consider the intraband transition using either the Boltzmann equation or the Drude model.

B. Accounting for Drude Model in Time-Domain Analysis

Based on the Drude model

$$\tilde{\mathbf{j}}_g(\omega) = \tilde{\sigma}_g(\omega)\tilde{\mathbf{E}}(\omega) = \frac{\sigma_{\mathrm{dc}}}{1+j\omega\tau}\tilde{\mathbf{E}}(\omega). \tag{11}$$

By multiplying $1+j\omega\tau$ to both sides and replacing the $j\omega$ with $\partial/\partial t$, the equation for $\mathbf{j}_g(t)$ in the time domain can be found as

$$\mathbf{j}_g(t) + \tau\frac{\partial \mathbf{j}_g(t)}{\partial t} = \sigma_{\mathrm{dc}}\mathbf{E}(t). \tag{12}$$

Using a backward difference to discretize the time derivative, we obtain

$$\{j_g\}^{n+1} + \tau\frac{\{j_g\}^{n+1} - \{j_g\}^n}{\Delta t} = \sigma_{\mathrm{dc}}\{e\}^n \tag{13}$$

from which we have the following time-domain update equation for the current density in graphene:

$$\{j_g\}^{n+1} = \left(\sigma_{\mathrm{dc}}\{e\}^n + \frac{\tau}{\Delta t}\{j_g\}^n\right)\Big/\left(\frac{\tau}{\Delta t}+1\right) \tag{14}$$

which is, then, used in conjunction with the FDTD to simulate Cu-G interconnects.

C. Drude Model in Conjunction With the FDTD Algorithm for Simulating On-Chip Cu-G Hybrid Interconnects

The electrical performance of a Cu-G interconnect is governed by the following Maxwell's equations from dc to high frequencies:

$$\nabla \times \mathbf{E} = -\mu\frac{\partial \mathbf{H}}{\partial t} \tag{15a}$$

$$\nabla \times \mathbf{H} = \epsilon\frac{\partial \mathbf{E}}{\partial t} + \sigma\mathbf{E} + \mathbf{j}_i \tag{15b}$$

where $\mathbf{E}$ is electric field intensity, $\mathbf{H}$ is magnetic field intensity, $\mathbf{j}_i$ is input (supply) current density, μ, ϵ, and σ are permeability, permittivity, and conductivity, respectively.

In this article, we apply an implicit unconditionally stable time-domain scheme developed in [20] to an FDTD-based discretization of Maxwell's equations. In this method, we discretize Maxwell's equations (15) as

$$\mathbf{S}_e\{e\}^{n+1} = -\mathbf{D}_\mu\frac{\{h\}^{n+\frac{1}{2}} - \{h\}^{n-\frac{1}{2}}}{\Delta t} \tag{16a}$$

$$\mathbf{S}_h\{h\}^{n+\frac{1}{2}} = \mathbf{D}_\epsilon\frac{\{e\}^{n+1} - \{e\}^n}{\Delta t} + \mathbf{D}_\sigma\{e\}^{n+1} + \{j_g\}^{n+1} + \{j_i\}^{n+1} \tag{16b}$$

where $\{e\}^n$ represents the vector of electric fields at the nth time instant, $\{h\}^{n+\frac{1}{2}}$ represents the vector of magnetic fields at the $n+\frac{1}{2}$ time instant, and $\{j_g\}^{n+1}$ represents the vector of conduction current densities in graphene layers, which is obtained from (14). In (16), $\{j_i\}$ denotes a vector of input current densities $\mathbf{D}_\mu$, $\mathbf{D}_\epsilon$, and $\mathbf{D}_\sigma$ are diagonal matrices of permeability, permittivity, and conductivity (for the nongraphene region), respectively. The matrix-vector products $\mathbf{S}_e\{e\}$ and $\mathbf{S}_h\{h\}$ represent discretized $\nabla \times \mathbf{E}$ and $\nabla \times \mathbf{H}$. The $\mathbf{S}_e$ and $\mathbf{S}_h$ can be readily constructed using a single-grid patch-based FDTD formulation developed in [21].

The Drude-model-based simulation algorithm is realized by substituting the current density $\{j_g\}^{n+1}$ in (14) into the right-hand side of Maxwell solver (16). The procedure, written in a pseudocode, is shown in Algorithm 1.

Algorithm 1: Drude Model + FDTD.

Set excitation and boundary conditions;
Initialize electromagnetic fields $\{e\}^1$ & $\{h\}^{\frac{1}{2}}$;
for *time step* $n := 1$ *to* n_{max} **do**
  Update $\{j_g\}^{n+1}$ with $\{j_g\}^n$ & $\{e\}^n$;
  Update $\begin{bmatrix}\{e\}^{n+1}\\ \{h\}^{n+\frac{1}{2}}\end{bmatrix}$ with $\begin{bmatrix}\{e\}^{n}\\ \{h\}^{n-\frac{1}{2}}\end{bmatrix}$ & $\{j_g\}^{n+1}$;
end

III. First-Principles-Based Multiphysics Modeling and Simulation of Cu-G Hybrid Interconnects

As shown in previous section, a Drude-model-based simulation relies on a few simplifications, which can miss the dynamic nonlinear physics at high frequencies, including both the nonlinear buildup of the conduction current in graphene and the nonlinear coupling between the electric field and electrons inside graphene layers. Therefore, an accurate model requires a direct observation of the charge carriers in graphene, thereby requires a direct solution of the charge carrier distribution function $f(\mathbf{r}, \mathbf{k}, t)$ through Boltzmann transport equation (1). In this section, we present a first-principles-based multiphysics modeling and simulation algorithm, cosimulating directly in the time-domain Maxwell's equations, equations characterizing graphene materials, and Boltzmann equation from dc to high frequencies, the preliminary work of which is shown in our conference paper [15]. This algorithm has also been validated through extensive numerical experiments and comparisons with measurements as shown in [16].

A. First-Principles-Based Multiphysics Modeling and Simulation Algorithm

The system of equations, which governs the electrical performance of Cu-G interconnects, consists of three sets of first-principle equations, namely Maxwell's equations (15), Boltzmann equation (1), and the dispersion relation of graphene (4). Because the carrier distribution function f is a function of $\mathbf{r}$, $\mathbf{k}$, and t, the computational domain for this model has seven dimensions in a 3-D analysis and five dimensions in a 2-D analysis. A flow of the cosimulation of these equations in the time domain is illustrated in Fig. 1. At the beginning, the charge carrier distribution $f(\mathbf{r}, \mathbf{k}, t)$ is initialized as equilibrium Fermi–Dirac distribution (2) for every spatial point in graphene, and the electromagnetic fields are initialized as 0. Then, at every time instant, given an external source, Maxwell's equations (15) are solved to obtain electric field $\mathbf{E}(\mathbf{r}, t)$, using which Boltzmann equation (1) can be solved to obtain charge carrier distribution $f(\mathbf{r}, \mathbf{k}, t)$. By integrating $f(\mathbf{r}, \mathbf{k}, t)$ over $\mathbf{k}$-space as shown in (3), the conduction current density $\mathbf{j}_g(\mathbf{r}, t)$ in graphene layers can be calculated at each space point. At next time instant, the graphene's conduction current density term $\sigma\mathbf{E}$ in Maxwell's equations (15) is replaced by latest $\mathbf{j}_g(\mathbf{r}, t)$, while the conduction current density in other conducting materials is still updated using $\sigma\mathbf{E}$. Now, with all the current terms updated, Maxwell's equations (15) are ready to be solved for next time instant. The whole process continues until a desired time is reached or until the physical phenomenon happening in a Cu-G interconnect has reached its steady state.

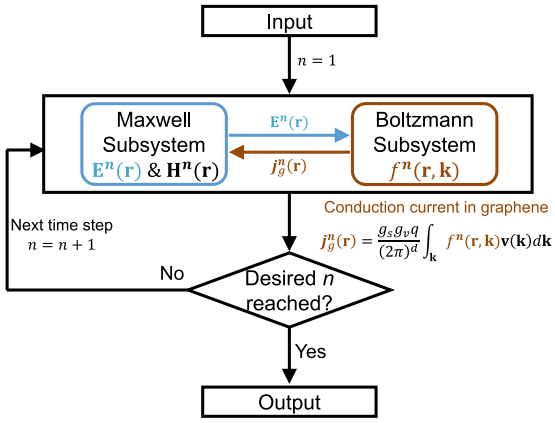

Fig. 1. Flowchart of the proposed multiphysics simulation algorithm, where the electromagnetic fields $\mathbf{E}$ and $\mathbf{H}$ and dynamic charge distribution f are updated at every time step.

We also develop an unconditionally stable time marching scheme to remove the dependence of time step on space step for an efficient simulation of the multiscaled and multiphysics system. The numerical solver for the Maxwell subsystem is already shown in (16). For the Boltzmann subsystem, substituting (5) into (1), the 2-D Boltzmann equation for graphene in the 4-D phase space $(x - y - k_x - k_y)$ becomes

$$\frac{v_{\mathrm{F}}}{k}\left(k_x\frac{\partial f}{\partial x} + k_y\frac{\partial f}{\partial y}\right) + \frac{q}{\hbar}\left(E_x\frac{\partial f}{\partial k_x} + E_y\frac{\partial f}{\partial k_y}\right) + \frac{\partial f}{\partial t} = -\frac{f - f_0}{\tau}. \tag{17}$$

Having $\nabla_{\mathbf{r}}$ and $\nabla_{\mathbf{k}}$ discretized with the central difference in the phase space, the remaining $\partial/\partial t$ could be discretized in time with a backward difference to guarantee the unconditional stability. As a result, we obtain

$$(\mathbf{S}_r + \mathbf{S}_k^n)\{f\}^{n+1} + \frac{\{f\}^{n+1} - \{f\}^n}{\Delta t} = \frac{\{f_0\} - \{f\}^{n+1}}{\tau} \tag{18}$$

where $\{f\}^n$ is the vector of carrier distribution function at the nth time instant, $\mathbf{S}_r\{f\}$ and $\mathbf{S}_k^n\{f\}$ represent discretized $\mathbf{v}\cdot\nabla_{\mathbf{r}}f$ and $\frac{q}{\hbar}\mathbf{E}\cdot\nabla_{\mathbf{k}}f$, respectively. Here, the superscript n of $\mathbf{S}_k^n$ denotes the time instant of $\mathbf{E}$ used to obtain $\mathbf{S}_k^n$. The grid used for discretizing the Maxwell's equations is also used for solving the Boltzmann subsystem, and the f is assigned at the $\mathbf{H}$'s points. The electric field $\mathbf{E}$ used in the Boltzmann equation is center averaged by neighboring $\mathbf{E}$ fields in the grid. The matrix-based expression, here, follows a similar logic as that in the Maxwell subsystem. The proposed time-marching formula for the Boltzmann subsystem (18) can be written as

$$\mathbf{B}^n\{f\}^{n+1} = \{f\}^n + \{\tilde{f}_0\} \tag{19}$$

where the constant term $\{\tilde{f}_0\} = \{f_0\}\Delta t/\tau$ and the system matrix

$$\mathbf{B}^n = \mathbf{I} + \Delta t/\tau + \Delta t(\mathbf{S}_r + \mathbf{S}_k^n). \tag{20}$$

As for the coupling between the Maxwell subsystem and the Boltzmann subsystem, the Boltzmann subsystem directly uses the electric field intensity $\mathbf{E}$ from the Maxwell subsystem, whereas the Maxwell subsystem uses, indirectly from the Boltzmann subsystem, the conduction current density $\{j_g\}^n$ in graphene layers. The $\{j_g\}^n$ is evaluated from $\{f\}^n$ through the integration of (3), which is numerically evaluated from a trapezoidal integration rule in the truncated $\mathbf{k}$-space. The numerical trapezoidal integration could also be expressed by a matrix-vector product of $\{j_g\}^n_{\text{2D}} = \mathbf{S}_{j\text{del}_2 D_{\text{2D}}}\{f\}^n$. The $\{j_g\}^n_{\text{2D}}$, here, is a surface current density, which agrees with the fact that graphene is a 2-D material whose current flow is a sheet current flow. However, Maxwell's equations require a volume current density $\{j_g\}^n$. Here, we can treat a graphene layer as a thin sheet [7] and obtain an equivalent volume current density $\{j_g\}^n = \{j_g\}^n_{\text{2D}}/dz$, [22] where dz is the grid size perpendicular to the graphene sheet. Thus, by using $\mathbf{S}_j = \mathbf{S}_{j\text{del}_2 D_{\text{2D}}}/dz$, we obtain

$$\{j_g\}^n = \mathbf{S}_j\{f\}^n. \tag{21}$$

The coupled systems of equations, including the Maxwell subsystem (16), the Boltzmann subsystem (19), and the coupling mechanism through conduction current density (21), constitute a nonlinear system of equations, as shown in the following:

$$\begin{bmatrix} \mathbf{M_A} & 0 \\ 0 & \mathbf{B}^n \end{bmatrix} \begin{bmatrix} \{x\}^{n+1} \\ \{f\}^{n+1} \end{bmatrix} = \begin{bmatrix} \mathbf{M_B} & \mathbf{M}_j \\ 0 & \mathbf{I} \end{bmatrix} \begin{bmatrix} \{x\}^{n} \\ \{f\}^{n} \end{bmatrix} + \begin{bmatrix} \{x_0\}^{n+1} \\ \{\tilde{f}_0\} \end{bmatrix} \tag{22}$$

where

$$\{x\}^n = \begin{bmatrix} \{e\}^n \\ \{h\}^{n-\frac{1}{2}} \end{bmatrix}$$

and

$$\mathbf{M}_A = \begin{bmatrix} \frac{\mathbf{D}_\epsilon}{\Delta t} + \mathbf{D}_\sigma & -\mathbf{S}_h \\ \mathbf{S}_e & \frac{\mathbf{D}_\mu}{\Delta t} \end{bmatrix} \text{ and } \mathbf{M}_B = \begin{bmatrix} \frac{\mathbf{D}_\epsilon}{\Delta t} & 0 \\ 0 & \frac{\mathbf{D}_\mu}{\Delta t} \end{bmatrix}$$

$$\mathbf{M}_j = \begin{bmatrix} -\mathbf{S}_j \\ 0 \end{bmatrix} \text{ and } \{x_0\}^{n+1} = \begin{bmatrix} -\{j_i\}^{n+1} \\ 0 \end{bmatrix}.$$

Given an initial condition $\{x\}^0$ and $\{f\}^0$, and the excitation $\{x_0\}$, we can update the system in time based on (22), and obtain a first-principles-based response of general 3-D Cu-G hybrid nanointerconnects.

In [16], we provide a detailed proof on the unconditional stability of the whole time marching system (22) regardless of the choice of time step. The unconditional stability of the entire system allows both Maxwell and Boltzmann subsystems to use the same arbitrary time step for time marching, despite their disparate characteristic time constants. Hence, the time step can be chosen solely based on accuracy. For the Boltzmann subsystem, the relaxation time approximation in Boltzmann equation (1) assumes an exponential decay with a relaxation time τ. Therefore, the physical process suggests the Boltzmann subsystem have a characteristic time constant τ. An accurate choice of time step in Boltzmann subsystem is, thus, one satisfying $\Delta t \leq \tau/10$. The characteristic time constant of Maxwell subsystem is usually determined by the maximum signal frequency ν_{sig}, which requires a $\Delta t \leq 1/(10\nu_{\text{sig}})$. As a result, for accuracy, the time step of the entire coupled system can be chosen as

$$\Delta t \leq \min\{\tau/10, 1/(10\nu_{\text{sig}})\}. \tag{23}$$

B. Comparison Between the First-Principles-Based Simulation and the Drude-Model-Based Simulation

The key difference between the first-principles-based simulation and the Drude-model based one is their way to deal with the conduction current in graphene. The first-principles model utilizes the dynamic time-domain response by directly solving Boltzmann equation (1), while the Drude model simplifies the Boltzmann transport theories to a steady-state conductivity model. The three major assumptions made in the Drude model may no longer be valid in simulating realistic ultra-scaled Cu-G hybrid nanointerconnects in a high-frequency setting, as revealed by the numerical examples shown in Section IV. Through extensive numerical experiments, we find that the spatial size and the signal frequency can determine the difference between the two simulations. First, a spatial size smaller than 100 nm can significantly increase the spatial variance of σ_{dc} extracted from a direct Boltzmann solver, thus, can decrease the reliability of ignoring the spatial variation term $\mathbf{v} \cdot \nabla_{\mathbf{r}} f$ in Boltzmann (1). Second, a high signal frequency, which is comparable to the back-scattering frequency of graphene, can lead to a nonlinear response, thus making the linear-response-based Drude model less accurate. The effect of simplifying f in $\mathbf{k}$-space is hard to distinguish in the comparison made here, because part of the effect is already included in σ_{dc}, and σ_{dc} in Drude model is provided from our direct Boltzmann solver.

IV. Numerical Results

In this section, we simulate a suite of examples to make a comparison between the first-principles-model-based simulation and the Drude model based one in analyzing Cu-G hybrid nanointerconnects. Numerical results indicate that two factors, spatial size and signal frequency, can determine the difference between the two simulations.

A. Validation of Both Simulations (First-Principles-Based and the Drude-Model-Based Simulations) at DC

The example is a graphene ribbon subject to a constant electric field, as shown in Fig. 2. In this case, the time-domain current density, from equilibrium state to steady state, has an analytical expression using the Drude model, as derived as follows. From the inverse Fourier transform, the time-domain counterpart of Drude model $\tilde{\sigma}_g(\omega) = \sigma_{\text{dc}}/(1 + j\omega\tau)$ can be found as

$$\sigma_g(t) = \frac{1}{2\pi}\int_{-\infty}^{+\infty} \frac{\sigma_{\text{dc}}}{1 + j\omega\tau} e^{j\omega t} d\omega = \frac{\sigma_{\text{dc}}}{\tau} e^{-t/\tau}. \tag{24}$$

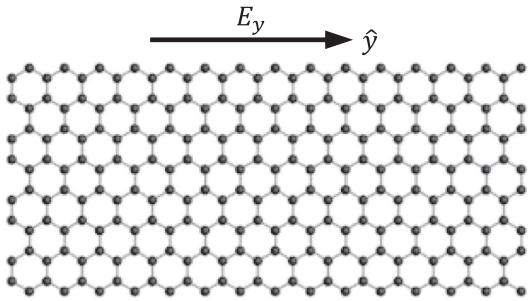

Fig. 2. Structure of a single layer graphene ribbon with length L and width W. The electric field E_y is applied along $\mathbf{y}$ direction.

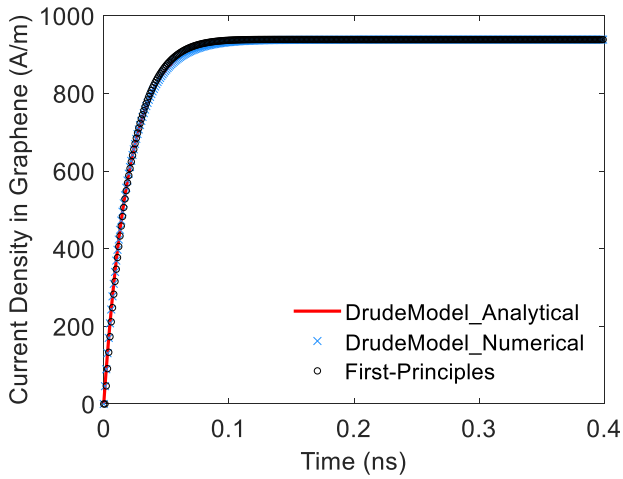

Fig. 3. Surface current density in a graphene layer subject to a constant electric field E_y.

Given a constant electric field $\mathbf{E}$, the time-domain current density in graphene layer is

$$\mathbf{j}_g(t) = \sigma_g(t) * \mathbf{E}(t) = \int_{-\infty}^{+\infty} \sigma_g(t-t')\mathbf{E}(t')dt'$$
$$= \int_0^t \frac{\sigma_{\rm dc}}{\tau} e^{-(t-t')/\tau}\mathbf{E}(t')dt' = \sigma_{\rm dc}\mathbf{E}(1-e^{-t/\tau}) \quad (25)$$

where $*$ denotes convolution. The above-mentioned equation can be used as a benchmark to validate both the numerical Drude-model-based simulator and the first-principles-based simulator developed in this article.

In this example, initial f is Fermi–Dirac distribution (2), Fermi energy $\xi_{\rm F} = 0.21$ eV, relaxation time $\tau = 4 \times 10^{-11}$ s, the electric field $E_y = 2 \times 10^3$ V/m, $dx = 5.4$ μm, and $dy = 5$ μm. Both simulators use the same $dt = 1 \times 10^{-12}$ s. After performing the time marching, it is found that the current densities obtained from both simulators, as shown in Fig. 3, agree very well with each other, and also with the analytical data.

Another feasible validation example is to find the surface dc conductivity $\sigma_{\rm dc\_2d}$ of a graphene sheet. Although the model developed in this article aims at the high-frequency and nonlinear responses of graphene, the solver can also accurately reproduce the measured $\sigma_{\rm dc\_2d}$. One measurement reports a $\sigma_{\rm dc\_2d} = 0.015$ S [13] for a graphene sheet of Fermi energy $\xi_{\rm F} = 0.21$ eV, mean free path $l = 600$ nm, therefore, relaxation time $\tau = l/v_{\rm F} = 6 \times 10^{-13}$ s. After substituting these parameters into the simulation result shown in Fig. 3, and dividing the steady-state surface current density j_y by the constant electric field E_y, the proposed Boltzmann solver gives a simulated $\sigma_{\rm dc\_2d} = 0.0147$ S, which agrees very well with the measurements since the relative error is only 2.0%.

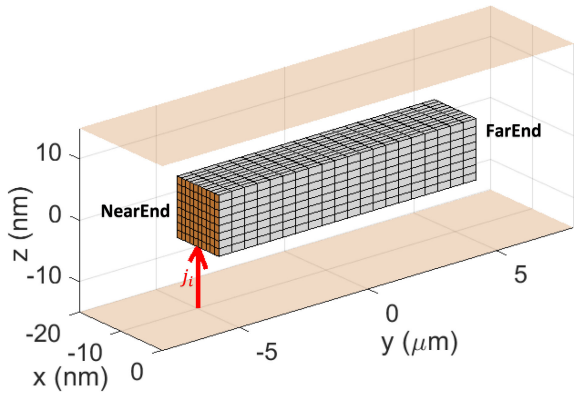

Fig. 4. Geometry and discretization of a Cu-G nanointerconnect. The cross section of the nanointerconnect is 10 nm $\times$ 10 nm. Port voltages at the near and far end are sampled for analysis.

B. Analysis of Graphene-Encapsulated Cu Nanointerconnects and Comparisons Between First-Principles-Based Simulation and Drude-Model-Based Simulation

A Cu-G nanointerconnect encapsulated by a single graphene layer on the top, left, and right sides [1] is simulated, whose geometry and discretization are illustrated in Fig. 4. The Cu interconnect, with $W = 10$ nm, $H = 10$ nm, and $L = 10$ μm, is discretized into a uniform $10 \times 8 \times 20$ grid. Graphene layers have a relaxation time $\tau = 2 \times 10^{-11}$ s and a Fermi energy $\xi_{\rm F} = 0.21$ eV, based on which we truncate the effective $\mathbf{k}$-space into an energy range from 0 to $2\xi_{\rm F}$. Then, we discretize the truncated 2-D $\mathbf{k}$-space with 10×20 grid cells. The extracted surface conductivity of graphene is $\sigma_{\rm dc\_2d} = 0.2286$ S. The Maxwell computation domain is a box with perfect electric conductor (PEC) boundaries at the top and the bottom, and PMC boundaries at the other four sides. For the aforementioned real space grid, due to the small spatial feature, conventional conditionally stable methods require about 10^7 time steps to finish the simulation of the Maxwell subsystem, and 10^9 time steps to simulate the Boltzmann subsystem in the window of a full pulse [23]. However, using the proposed unconditionally stable algorithm, only 200 time steps are required, where time step is solely determined by accuracy as given by (23). Furthermore, the same time step is used for simulating both Maxwell and Boltzmann subsystems.

From extensive numerical experiments, we find propagation delay and voltage drop are good metrics to demonstrate the difference between a first-principles-based simulation and a simplified-model-based simulation. Moreover, in the following

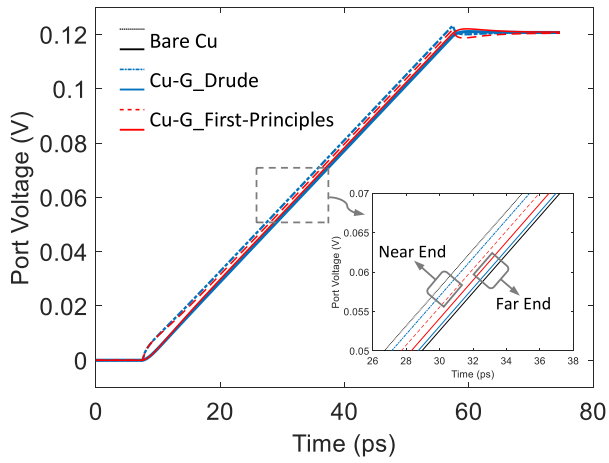

(a)

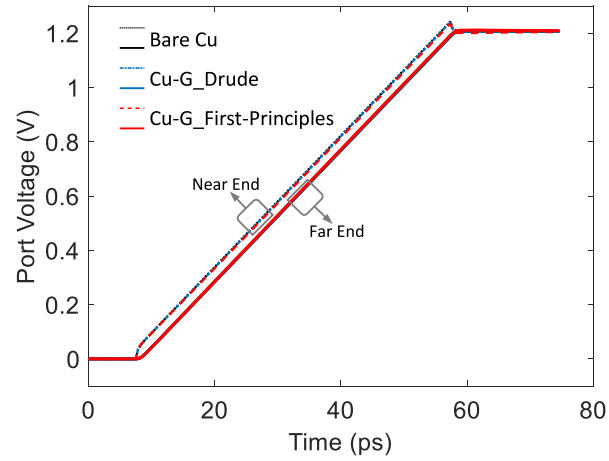

(b)

Fig. 5. Near- and far-end port voltages of a Cu-G nanointerconnect. The red color is from the first-principles-based multiphysics simulation, the blue color is from the Drude-model-based simulation, and the black color is from the simulation of Bare Cu counterparts without graphene coating. All solid lines represent far-end voltages while dashed and dotted lines represent near-end voltages. (a) Simulation of the Cu-G nanointerconnect in Fig. 4. (b) Simulation of a 10 times larger version of the Cu-G interconnect in Fig. 4.

numerical examples, we also use the propagation delay and voltage drop to show how the spatial size and the signal frequency change the difference between two simulations.

1) Determining Factor 1-Feature Size: We first analyze the propagation delay in the Cu-G nanointerconnect by injecting a current source of

$$j_i(t) = \begin{cases} 1.09 \times 10^{10}\ \text{A/m}^2 & 7.5\ \text{ps} < t < 57.5\ \text{ps} \\ 0 & \text{otherwise.} \end{cases}$$

The resulting port voltages, given in Fig. 5, has a rising time of 50 ps. To show the effect of spatial size, a small example of 10 nm $\times$ 10 nm $\times$ 10 μm and a larger example of 100 nm $\times$ 100 nm $\times$ 100 μm are simulated. The small example has a structure shown in Fig. 4. Its port voltages are plotted in Fig. 5(a). For the larger example in Fig. 5(b), only the spatial size is enlarged by 10 times and all the other settings are the same

TABLE I
PROPAGATION DELAY PREDICTED BY THE FIRST-PRINCIPLES-BASED SIMULATION AND THE DRUDE-MODEL-BASED ONE

Feature Size	Bare Cu	Cu-G, Drude	Cu-G, First-Principles
10 nm$\times$10 nm$\times$10 μm	2.2513 ps	1.5830 ps	0.5864 ps
100 nm$\times$100 nm$\times$100 μm	2.2513 ps	2.1201 ps	1.8476 ps

as in the small example. The simulated propagation delays from two simulations are listed in Table I. For the small example, the Drude model gives a propagation delay three times larger than the first-principles-based multiphysics simulation. For the larger example, the difference between two simulations becomes much smaller. More experiments show that 100 nm is a good separation criterion, above which two simulations give almost the same results, whereas below 100 nm two simulations can be very different. Direct observations on the extracted σ_{dc} of the graphene plane show a large spatial variation when the spatial size is smaller than 100 nm. However, when the spatial size is larger than 100 nm, the extracted σ_{dc} is identical everywhere in the graphene plane. As analyzed previously, a major difference between two simulations is the Drude model's ignoring the spatial variation term $\mathbf{v} \cdot \nabla_{\mathbf{r}} f$ in Boltzmann (1).

2) Determining Factor 2-Signal Frequency: To show the effect of a high signal frequency, a Gaussian derivative source current density is injected from the near end of the structure in Fig. 4. The Gaussian derivative pulse has a relatively narrow frequency band, which helps the analysis of the difference between the two simulations. For the injected source current, it has a waveform of $j_i = -(t - t_0)\exp[-(\frac{t-t_0}{\tau_s})^2] \times 10^{16}$ A/m^2, where $t_0 = 4\tau_s$ and $\tau_s = 2 \times 10^{-11}$ s, the maximal signal frequency of which is approximately 50 GHz. Here, the relaxation time of graphene is still $\tau = 2 \times 10^{-11}$ s, yielding a back scattering frequency of 50 GHz and a surface dc conductivity $\sigma_{\text{dc\_2d}} = 0.2286$ S. The source current and the voltage drop along the single graphene-encapsulated Cu nanointerconnect are plotted in Fig. 6(a).

As can be seen from the waveform of voltage drops in Fig. 6(a), Drude-model-based simulation predicts a Gaussian derivative voltage drop that is the same as the waveform of the source current, therefore, indicates a pure resistor-like performance. However, the first-principles model shows an oscillating voltage drop, therefore, predicts a full-wave effect for the graphene-encapsulated Cu nanointerconnect. As for the low-frequency comparison, one example at dc is already shown in Fig. 3, where the Drude model agrees very well with the first-principles solver.

The reason to the difference caused by a high signal frequency is much more complicated than that caused by the spatial factor. First, Drude model assumes a linear coupling between the Maxwell and Boltzmann subsystems by using Ohm's Law (11). However, this is unlikely to be the case. For example, the nonlinear operation (3), an integration of f over $\mathbf{k}$-space to obtain the current, can directly cause the nonlinear coupling between the Maxwell and Boltzmann subsystems. Second, Drdue model assumes a linear response in Boltzmann equation by replacing $\partial/\partial t$ with $j\omega$. The Boltzmann equation has its own characteristic frequency ω_{BE} determined by the relaxation time τ, which tells

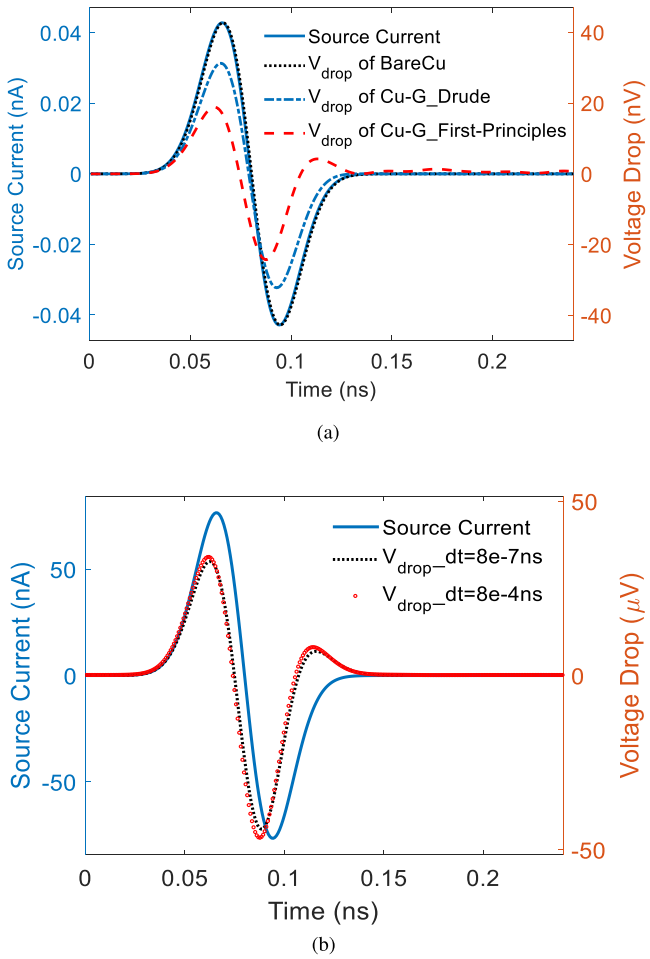

Fig. 6. Time-domain voltage drop (labeled to the right) along the single Graphene-encapsulated Cu nanointerconnect in Fig. 4. The Gaussian derivative source current is plotted in solid line and labeled to the left. (a) Comparison between different models. (b) Comparison between different choice of time step in the proposed first-principles modeling.

how f attenuates to its steady state. When the signal frequency ω_{sig}, namely the characteristic frequency of Maxwell subsystem and the electric field, is comparable to the ω_{BE}, the electric field changes so fast that the f can hardly attenuate to its steady state. As a result, the response of f, governed by Boltzmann equation (1), is not linear. At a high signal frequency, both of the two reasons given previously can be important, making the Drude model less accurate. However, at a low frequency, the two factors are less important as the electric field changes very slowly. Thus, the Boltzmann equation is subject to an almost constant electric field, giving a linear response and linear coupling. That is why, we see a good match between two simulations at a low frequency. The same analysis can be applied to many other steady-state models of graphene.

We also simulated this example using the time step permitted by a conditionally stable scheme, and investigated whether our unconditionally stable method is able to produce the same accurate result while using an orders-of-magnitude larger time step. As can be seen from Fig. 6(b), they do agree well with each other. In this figure, the conventional method uses a time step of 8×10^{-7} ns, while the proposed one uses 8×10^{-4} ns.

V. Conclusion

In this article, we develop two modeling and simulation algorithms for analyzing the on-chip Cu-G hybrid nanointerconnects. One algorithm uses a simplified Drude model together with the FDTD, while the other is a multiphysics model cosimulating in the time-domain Maxwell's equations, Boltzmann equation under relaxation time approximation, and the linear dispersion of graphene. The differences between two algorithms are theoretically analyzed by examining the assumptions and simplifications made in the Drude model. Moreover, we also study the differences via numerical experiments performed on the graphene-encapsulated Cu nanointerconnects. From our analysis, an on-chip Cu-G hybrid system, featuring a high operating frequency and a sub-10 nm dimension, requires a more accurate first-principles-based modeling and simulation algorithm so that the dynamic coupling between graphene and electromagnetic fields can be accurately captured. In the future, more physical effects, such as the surface scattering at the Cu-G interface, can be included to enrich the multiphysics model and enhance its prediction power.

References

[1] R. Mehta, S. Chugh, and Z. Chen, "Enhanced electrical and thermal conduction in graphene-encapsulated copper nanowires," *Nano Lett.*, vol. 15, no. 3, pp. 2024–2030, Feb. 2015.
[2] A. Naeemi and J. D. Meindl, "Compact physics-based circuit models for graphene nanoribbon interconnects," *IEEE Trans. Electron Devices*, vol. 56, no. 9, pp. 1822–1833, Sep. 2009.
[3] V. P. Gusynin, S. G. Sharapov, and J. P. Carbotte, "Magneto-optical conductivity in graphene," *J. Phys. Condens. Matter*, vol. 19, no. 2, Dec. 2006, Art. no. 026222.
[4] G. W. Hanson, "Dyadic greens functions and guided surface waves for a surface conductivity model of graphene," *J. Appl. Phys.*, vol. 103, no. 6, Mar. 2008, Art. no. 064302.
[5] A. G. D. Aloia, W. Zhao, G. Wang, and W. Yin, "Near-field radiated from carbon nanotube and graphene-based nanointerconnects," *IEEE Trans. Electromagn. Compat.*, vol. 59, no. 2, pp. 646–653, Apr. 2017.
[6] V. Nayyeri, M. Soleimani, and O. M. Ramahi, "Modeling graphene in the finite-difference time-domain method using a surface boundary condition," *IEEE Trans. Antennas Propag.*, vol. 61, no. 8, pp. 4176–4182, Aug. 2013.
[7] R. M. S. d. Oliveira, N. R. N. M. Rodrigues, and V. Dmitriev, "FDTD formulation for graphene modeling based on piecewise linear recursive convolution and thin material sheets techniques," *IEEE Antennas Wireless Propag. Lett.*, vol. 14, pp. 767–770, 2015.
[8] A. Vakil and N. Engheta, "Transformation optics using graphene," *Science*, vol. 332, no. 6035, pp. 1291–1294, 2011.
[9] D. Sarkar, C. Xu, H. Li, and K. Banerjee, "High-frequency behavior of graphene-based interconnects-part I: Impedance modeling," *IEEE Trans. Electron Devices*, vol. 58, no. 3, pp. 843–852, Mar. 2011.
[10] R. Wang, X.-G. Ren, Z. Yan, L.-J. Jiang, W. E. I. Sha, and G.-C. Shan, "Graphene based functional devices: A short review," *Front. Phys.*, vol. 14, no. 1, Oct. 2018, Art. no. 13603.
[11] B. S.-Rodriguez *et al.*, "Broadband graphene terahertz modulators enabled by intraband transitions," *Nat. Commun.*, vol. 3, p. 780, 2012.
[12] J. Horng *et al.*, "Drude conductivity of dirac fermions in graphene," *Phys. Rev. B*, vol. 83, Apr. 2011, Art. no. 165113.
[13] C. Berger *et al.*, "Electronic confinement and coherence in patterned epitaxial graphene," *Science*, vol. 312, no. 5777, pp. 1191–1196, 2006.
[14] E. H. Hwang and S. D. Sarma, "Single-particle relaxation time versus transport scattering time in a two-dimensional graphene layer," *Phys. Rev. B*, vol. 77, May 2008, Art. no. 195412.
[15] S. Sun and D. Jiao, "Multiphysics modeling and simulation of 3-D Cu-Graphene hybrid nano-interconnects," in *Proc. IEEE MTT-S Int. Conf. Numer. Electromagn. Multiphys. Modeling Optim.*, May 2019, pp. 1–4.
[16] S. Sun and D. Jiao, "Multiphysics modeling and simulation of 3-D Cu-Graphene hybrid nanointerconnects," *IEEE Trans. Microw. Theory Tech.*, vol. 68, no. 2, pp. 490–500, Feb. 2020.

[17] C. Kittel, *Introduction to Solid State Physics*, 8th ed. Hoboken, NJ, USA: Wiley, 2005.
[18] H. Peng *et al.*, "Substrate doping effect and unusually large angle van hove singularity evolution in twisted Bi- and multilayer graphene," *Adv. Mater.*, vol. 29, no. 27, 2017, Art. no. 1606741.
[19] M. Jablan, H. Buljan, and M. Soljačić, "Plasmonics in graphene at infrared frequencies," *Phys. Rev. B*, vol. 80, Dec. 2009, Art. no. 245435.
[20] J. Yan and D. Jiao, "Time-domain method having a naturally diagonal mass matrix independent of element shape for general electromagnetic analysis—2-D formulations," *IEEE Trans. Antennas Propag.*, vol. 65, no. 3, pp. 1202–1214, Mar. 2017.
[21] J. Yan and D. Jiao, "Fast explicit and unconditionally stable FDTD method for electromagnetic analysis," *IEEE Trans. Microw. Theory Tech.*, vol. 65, no. 8, pp. 2698–2710, Aug. 2017.
[22] J. G. Maloney and G. S. Smith, "The efficient modeling of thin material sheets in the finite-difference time-domain (FDTD) method," *IEEE Trans. Antennas Propag.*, vol. 40, no. 3, pp. 323–330, Mar. 1992.
[23] S. Sun and D. Jiao, "Multiphysics simulation of high-speed graphene-based interconnects in time domain," in *Proc. IEEE Int. Symp. Antennas Propag.*, Jul. 2018, pp. 1169–1170.

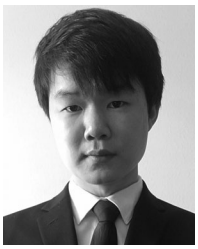

Shuzhan Sun (Graduate Student Member, IEEE) received the B.S. degree in physics from the School of Special Class for the Gifted Young, University of Science and Technology of China, Hefei, China, in 2016, and the M.S. degree in physics in 2018 from the On-Chip Electromagnetics Group, Purdue University, West Lafayette, IN, USA, where he is currently working toward the Ph.D. degree in electrical and computer engineering.

His current research interests include simulating next-generation Cu-graphene hybrid nanointerconnects and developing novel electromagnetic algorithms for large-scale simulation.

Mr. Sun was a Best Student Paper Award finalist at the IEEE International Symposium on Antennas and Propagation in 2019.

Dan Jiao (Fellow, IEEE) received the Ph.D. degree in electrical engineering from the University of Illinois at Urbana-Champaign, Champaign, IL, USA, in 2001.

She was with the Technology Computer-Aided Design (CAD) Division, Intel Corporation, until September 2005, as a Senior CAD Engineer, Staff Engineer, and Senior Staff Engineer. In September 2005, she joined Purdue University, West Lafayette, IN, USA, as an Assistant Professor with the School of Electrical and Computer Engineering, where she is currently a Professor. She has authored three book chapters and more than 260 papers in refereed journals and international conferences. Her current research interests include computational electromagnetics, high-frequency digital, analog, mixed-signal, and RF integrated circuit (IC) design and analysis, high-performance VLSI CAD, modeling of microscale and nanoscale circuits, applied electromagnetics, fast and high-capacity numerical methods, fast time-domain analysis, scattering and antenna analysis, RF, microwave, and millimeter-wave circuits, wireless communication, and bio-electromagnetics.

Dr. Jiao has been a reviewer for many IEEE journals and conferences. She is an Associate Editor for the IEEE TRANSACTIONS ON COMPONENTS, PACKAGING, AND MANUFACTURING TECHNOLOGY and an Associate Editor for the IEEE JOURNAL ON MULTISCALE AND MULTIPHYSICS COMPUTATIONAL TECHNIQUES. She received the 2013 S. A. Schelkunoff Prize Paper Award of the IEEE Antennas and Propagation Society, which recognizes the Best Paper published in the IEEE TRANSACTIONS ON ANTENNAS AND PROPAGATION during the previous year. She was among the 21 women faculty selected across the country as the 2014–2015 Fellow of Executive Leadership in Academic Technology and Engineering, Drexel, a national leadership program for women in the academic STEM fields. She has been named a University Faculty Scholar by Purdue University since 2013. She was among the 85 engineers selected throughout the nation for the National Academy of Engineerings 2011 US Frontiers of Engineering Symposium. She was the recipient of the 2010 Ruth and Joel Spira Outstanding Teaching Award, the 2008 National Science Foundation CAREER Award, the 2006 Jack, and Cathie Kozik Faculty Start up Award (which recognizes an outstanding new faculty member of the School of Electrical and Computer Engineering, Purdue University), a 2006 Office of Naval Research Award under the Young Investigator Program, the 2004 Best Paper Award presented at the Intel Corporations annual corporate-wide technology conference (Design and Test Technology Conference) for her work on generic broadband model of high-speed circuits, the 2003 Intel Corporations Logic Technology Development Divisional Achievement Award, the Intel Corporations Technology CAD Divisional Achievement Award, the 2002 Intel Corporations Components Research the Intel Hero Award (Intel-wide she was the tenth recipient), the Intel Corporations LTD Team Quality Award, and the 2000 Raj Mittra Outstanding Research Award presented by the University of Illinois at Urbana-Champaign.